ISSN 0036-0244, Russian Journal of Physical Chemistry A, 2022, Vol. 96, No. 2, pp. 371–380. © Pleiades Publishing, Ltd., 2022.

PHYSICAL CHEMISTRY OF NANOCLUSTERS AND NANOMATERIALS

Removal of Methylene Blue Dye from Aqueous Solutions Using Carboxymethyl-β-Cyclodextrin-Fe_3O_4 Nanocomposite: Thermodynamics and Kinetics of Adsorption Process

Hediyeh Sadat Ghazimokri[a,*], Hossein Aghaie[a,], Majid Monajjemi[b], and Mohammad Reza Gholami[c]**

[a] *Department of Chemistry, Science and Research Branch, Islamic Azad University, Tehran, Iran*

[b] *Department of Chemical Engineering, Central Tehran Branch, Islamic Azad University, Tehran, Iran*

[c] *Sharif University of Technology, Tehran, Iran*

** e-mail: h.ghazimokri@gmail.com*

*** e-mail: hn_aghaie@yahoo.com, h.aghaei@srbiau.ac.ir*

Received December 14, 2020; revised February 1, 2021; accepted February 5, 2021

Abstract—The applicability of the synthesized carboxymethyl-β-cyclodextrin-Fe_3O_4 nanocomposite (CM-β-CD-Fe_3O_4NPs) as a novel adsorbent for eliminating Methylene blue dye (MB) from aqueous media was investigated. Various techniques including Brunauer Emmett Teller analysis (BET), Fourier transform infrared spectroscopy (FT-IR), X-ray diffraction (XRD), scanning electron microscopy (SEM), and transmission electron microscopy (TEM) have been used to characterize this novel adsorbent. The effect of initial concentration (C_0), pH, adsorbent dosage (dose), contact time (t_c), and temperature (T, K) on the removal percentage (Ad%) of MB dye onto CM-β-CD-Fe_3O_4NPs was studied, and the optimum value of each factor was determined (pH 6.0, dose = 0.20 g, t_c = 45.0 min, and T = 298.0 K). Several isotherm models, such as Langmuir, Freundlich and Redlich–Peterson models were used to represent the adsorption experimental results, but the Freundlich model represents better the results than others. The pseudo-second-order kinetics coincided quite with the kinetic results. Based on the obtained thermodynamic values such as standard Gibbs free energy change ($\Delta G^\circ_{ad} < 0$), standard enthalpy change ($\Delta H^\circ_{ad} < 0$) and standard entropy change ($\Delta S^\circ_{ad} < 0$), the nature of the adsorption process was spontaneous, exothermic and mainly physisorption.

Keywords: adsorption, removal percentage, isotherm model, adsorption kinetics, adsorption thermodynamics

DOI: 10.1134/S0036024422020108

1. INTRODUCTION

Pollution control and economical limitations have been one of the major concerns of global leaders over the last few decades. Dye untreated wastewater discharged from textile and dyestuff industries are important sources of contamination and have toxic or harmful effects on ecosystems and environment. Among all the organic material, removing colors are the hardest and most complicated [1]. Colors are the first known pollutions which must be omitted from aqueous solutions, before discharging them to the wastewater [2]. Dyes and pigments have been extensively released in the wastewaters from different industries, particularly from textile, paper, rubber, plastic, leather, cosmetic, food, and drug industries. These dyes can cause allergic dermatitis, skin irritation, cancer and mutation in living organisms. It also causes eye burns, which may be responsible for permanent injury to the eyes of human and animals. On inhalation, it can give rise to short periods of rapid or difficult breathing, while ingestion through the mouth produces a burning sensation and may cause nausea, vomiting, profuse sweating, mental confusion, painful micturition, and methemoglobinemia-like syndromes [3]. Because of their synthetic natures and complex aromatic molecular structures, dyes are almost non-biodegradable in the ecosystem. The importance of the potential pollution of dyes and their intermediates has been incited with the toxic nature of many dyes, different mutagenic effects, skin diseases and skin irritation and allergies. Moreover, they are dangerous because their microbial degradation compounds, such as benzidine or other aromatic compounds have carcinogenic effect [4, 5]. The existence of the dyes in water, even at very low dosage, is extremely undesirable.

Cationic dye, methylene blue ($C_{16}H_{18}ClN_3S$) is widely used by industries [6]. At dosages exceeding 5 mg/kg, MB may precipitate serious serotonin toxicity, serotonin syndrome. Some of the by far known side effects of MB are mild bladder irritation, dizziness, headache, sweating, nausea/vomiting, diarrhea, frequent urination or stomach cramps. Lots of meth-

ods have been investigated and applied for the removal of the hazardous dyes from wastewater [7]. One of the most promising method is to use activated carbons which are not eco-friendly and almost cost-effective advancement [8]. Therefore, many researchers have used different methods to treat the dye wastewater [9].

Adsorption is one of the best and simple techniques for the removal of toxic and noxious impurities in comparison to other conventional protocols such as flocculation, membrane filtration, advanced oxidation, ozonation, photocatalytic degradation, and biodegradation [10]. These traditional methods have inherent limitations [10] such as the complex and uneconomical of nature of the technology, and thus it is necessary to seek efficient and simple dye wastewater treatment methods [11]. Iron oxide nanoparticles are widely used for metal remediation due to their low toxicity and easy separation from water media [12, 13], in addition, where the nanoparticle (NP) is composed of magnetite, a facile magnetic separation of NPs, along with associated contaminants, can be performed. However, bare magnetite nanoparticles rapidly aggregate in aqueous systems and are highly susceptible to transformations under many environmental conditions [14, 15]. Among these methods, nanomaterial's based adsorbents are highly recommended for dyes pollutants removal [16]. The efficient applicability of an adsorption process mainly depends on the physical and chemical characteristics of the adsorbent, which is expected to have high adsorption capacity and to be recoverable and available at economical cost. Currently, various potential adsorbents have been implemented for removal of specific organics from water samples. In this regard, magnetic nanoparticles (MNPs) have been studied extensively as novel adsorbents with large surface area, high adsorption capacity and small diffusion resistance. For instance, they have been used for separation of chemical species such as environmental pollutants, metals, dyes, and gases [17, 18].

Cyclodextrins (CD) are natural macroheterocycles that they are obtained by enzymatic digestion of starch. The α-, β-, and γ-cyclodextrins contain respectively 6, 7, and 8 glucopyranose units, with primary and secondary hydroxyl groups located on the narrow and wider rims of a truncated cone shape structure [19, 20]. The steric arrangement of glucose units in the CD molecule brings in the shape of a hollow truncated cone with a hydrophilic external surface and a hydrophobic internal cavity, which permits CDs to form inclusion complexes with different guest molecules [21]. The principal advantages of natural CDs as drug carriers are: (1) the availability of CDs of different cavity sizes, (2) a well-defined chemical structure, yielding many potential sites for chemical modification [22]. In recent years, researchers have made the ability of cyclodextrin nanocomposite due to the structural, chemical and biological stability of this nanocomposite to be a very good choice as a solid phase extraction adsorbent for water treatment applications and by placing magnetite nanoparticles (Fe_3O_4) inside of cyclodextrin, making it with a significant magnetic property that has many applications, especially as an effective adsorbent [23].

In the present study, after synthesizing CM-β-CD-Fe_3O_4NPs as a unique adsorbent, its characterization was performed by using FTIR, SEM, and XRD. In the process of MB dye removal, the effects of important variables such as contact time, pH of solution, adsorbent dosage, temperature, and MB dye initial concentration as well as the dye removal percentage were investigated [24, 25]. The pseudo-second-order rate equation matched quite the adsorption kinetics of MB dye adsorption and it was very evident. Also the Freundlich isotherm model could better fit the related results than other model and explaining better the adsorption equilibrium data. However the specific isotherm models such as Freundlich, Langmuir, and Redlich–Peterson were used to fit the experimental equilibrium data. But eventually the findings confirmed the suitability and applicability of the Freundlich model. Moreover, it was shown that the kinetics of the adsorption process was more favorable with pseudo-second-order equation than the pseudo-first-order or diffusion model equations. As a final result, the capability and usefulness of CM-β-CD-Fe_3O_4NPs for removing the MB dye from aqueous media were effectively proven.

2. EXPERIMENTAL

2.1. Preparation of Stock Solution

Methylene Blue dye, sodium hydroxide, hydrochloric acid, and the other necessary chemicals were supplied from Merck (Darmstadt, Germany), $FeCl_3{\cdot}6H_2O$ (>98%) was purchased from BDH and $FeCl_2{\cdot}4H_2O$ (98%) from Alfa Aesar. All used chemicals were of reagent grade and utilized without further purification. For the pH adjustment, HCl_{aq} (hydrochloric acid) and $NaOH_{aq}$ (sodium hydroxide) were applied.

2.2. Instruments

UV–Vis spectrophotometer (jasco, Model UV–Vis V-530, Japan). Fourier transform infrared (FT-IR) spectra was from PerkinElmer (FT-IR spectrometer BX, Germany). The morphology of samples was studied by scanning electron microscopy (SEM: KYKY-EM 3200, Hitachi Company, China) under an acceleration voltage of 26 kV). The pH/ion meter (model-728, Metrohm Company, Switzerland, Swiss) was used for pH measurements. Laboratory glassware was kept overnight in 10% nitric acid solution.

2.3. CM-β-CD-Fe_3O_4NPs Preparation

Initially a mixture of β-CD (2 g) and sodium hydroxide (1.86 g) in 7.5 mL distilled water was treated with 5.5 mL of monochloroacetic acid solution of 16.3% purity. The precipitated process was accomplished in the presence of sufficient methanol and the resultant mixture was dried under vacuum at 50°C to obtain CM-β-CD compound [26]. Then, CM-β-CD-Fe_3O_4NPs was briefly fabricated by mixing 0.86 g of $FeCl_2{\cdot}4H_2O$ with 2.35 g $FeCl_3{\cdot}6H_2O$ (mole rat of Fe^{2+} : Fe^{3+} = 1 : 2) and 1.5 g CM-β-CD in 40 mL of deoxygenated water under vigorous stirring at a speed of 500 rpm, while 40 mL of NH_4OH_{aq} (25%) was very slowly added to the obtained mixture. Afterward, the resultant product was heated under constant stirring and sufficient nitrogen flow (for removing oxygen from the experimental medium and protecting Fe_3O_4 against the critical oxidation) for 1 h at 80°C. The resultant CM-β-CD-Fe_3O_4NPs was washed several times with deionized water and then it was dried in a vacuum oven [27]. Finally, the prepared CM-β-CD-Fe_3O_4NPs was treated with a leaf medlar in an equal weight ratio and then it was characterized by BET, FT-IR, XRD, SEM, and TEM analysis.

2.4. A Typical Adsorption Experiment

Generally, batch method is currently used in adsorption studies [28]. This method includes the following steps: (1) selecting an adequate solution of adsorbate with a known initial concentration in a suitable container (e.g., 50.0 mL, C_0 = 25.0 mg/L). (2) Adding an adequate dosage of adsorbent to the previous solution (e.g., 0.20 g). (3) Adjusting pH and temperature on desirable values (e.g., 6.0 and 25.0°C). (4) Stirring the resultant mixture in step (3) for a suitable contact time (e.g., 40.0 min). (5) Separating the solid phase from the solution phase under the equilibrium state by an effective technique (e.g., centrifuge). (6) Measuring the concentration of the adsorbate in the remaining solution upon filtration by a suitable method (e.g., spectrophotometry). (7) Evaluating the removal percentage (Ad%) and adsorption capacity of the adsorbent (q_e) from the following equations:

$$\mathrm{Ad}\% = \frac{(C_0 - C_e)}{C_0} \times 100, \quad (1)$$

$$q_e = \frac{(C_0 - C_e)V}{w}, \quad (2)$$

$$q_t = \frac{(C_0 - C_t)V}{w}, \quad (3)$$

where C_0 is the initial dye concentration of the adsorbate (mg/L), C_e is the equilibrium dye concentration of the adsorbate (mg/L), and C_t is the dye concentration of the adsorbate at any time t (mg/L), w is the weight of the adsorbate (g), and V is the volume of the solution (L), Ad% is removal percentage or adsorption percent and the amount of adsorbed dye at equilibrium per gram of adsorbent, q_e, (mg/g), and at time t, q_t, (mg/g) [29, 30].

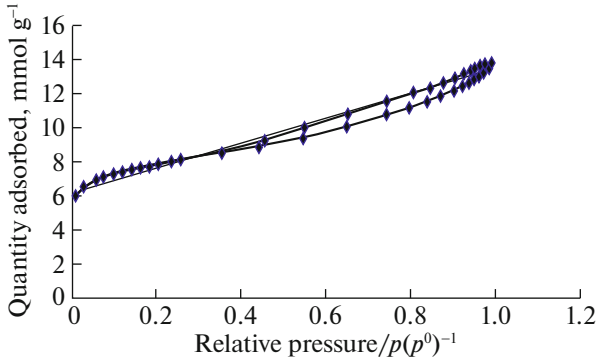

Fig. 1. Physisorption isotherms of N_2 onto CM-β-CD-Fe_3O_4NPs.

3. RESULTS AND DISCUSSION

3.1. Characterization of Adsorbent

3.1.1. BET analysis of CM-β-CD-Fe_3O_4NPs. The nitrogen adsorption–desorption isotherm at 77 K onto CM-β-CD-Fe_3O_4NPs is presented in Fig. 1. This isotherm is consistent with classical type III isotherm of IUPAC classification [31]. The porosity and chemical reactivity of functional groups at the surface control the adsorption capacity of CM-β-CD-Fe_3O_4NPs. Comprehensive knowledge of the surface functional groups would provide an overview of the adsorption potentiality of the CM-β-CD-Fe_3O_4NPs (Table 1).

3.1.2. FTIR analysis. The binding of CM-β-CD on surfaces of Fe_3O_4NPs has been confirmed by FTIR spectroscopy. Figure 2 shows the FTIR spectra of CM-β-CD and CM-β-CD-Fe_3O_4NPs in the 500–4000 cm^{-1} wave number range. As demonstrated in Fig. 2b, the FTIR spectrum of CM-β-CD-Fe_3O_4NPs presents clear peak at 569 cm^{-1} related to Fe–O. The novel emerging signal at 3433 cm^{-1} can be attributed to –OH stretching. The 2928 cm^{-1} band can be regarded as being caused by C–H stretching in CM-β-CD system, the peaks at 1053 and 1637 cm^{-1} corresponded to C–O–C and C–C bonds, and the one at 1704 cm^{-1} can be ascribed to C=O bonds which confirms the incorporation of the carboxymethyl group ($-COOCH_3$) into CM-β-CD molecule (Fig. 2a). All the significant peaks of CM-β-CD in the range of 900–1200 cm^{-1} are present in the spectrum of CM-β-CD-Fe_3O_4NPs with a small shift. As shown in Fig. 2b, it can be concluded that CM-β-CD has been grafted successfully on the surface of magnetic nano-adsorbent [32].

Table 1. BET characterization of CM-β-CD and CM-β-CD-Fe_3O_4NPs

Characterization		Samples	
		CM-β-CD	CM-β-CD-Fe_3O_4NPs
BET data	Surface area (m^2/g)	81.45	97.85
	Correlation coefficient	0.9982	0.9913
BJH adsorption summary	Surface area (m^2/g)	65.95	65.71
	Pore volume (cm^3/g)	0.384	0.381
	Pore diameter (Å)	98.52	98.21
BJH desorption summary	Surface area (m^2/g)	88.97	88.68
	Pore volume (cm^3/g)	0.431	0.428
	Pore diameter (Å)	56.38	56.23

3.1.3. XRD analysis. Figure 3 represents the X-ray diffraction of the CM-β-CD-Fe_3O_4NPs adsorbent and CM-β-CD. The peaks at 2θ = 28.17°, 30.2°, 34.21°, 37.2°, 43.2°, 53.6°, and 67.12° belong to the lattice planes of (111), (220), (311), (222), (400), (422), and (511), confirming the cubic structure of CM-β-CD-Fe_3O_4NPs. However, the great intensity of signal at 34.21° (311) confirmed that there is a slight amount of amorphous state material. Indeed, the perfect synthesis of CM-β-CD-Fe_3O_4NPs can be judged through looking at its XRD pattern.

3.1.4. Surface morphology. The morphological properties of CM-β-CD-Fe_3O_4NPs was investigated by SEM and is exhibited in Figs. 4a–4c. As demonstrated in Fig. 4c, the evenness, homogeneity, orderliness and approximate uniformity of synthesized CM-β-CD-Fe_3O_4NPs (even in size distribution) can be observed. CM-β-CD-Fe_3O_4NPs after surface modification came to be uneven, bigger and agglomerate. It can be seen that the particles are mostly spherical with the various size distribution as they form agglomerates. Based on the particle size distribution, we obtained the average particle size in the range of 40–60 nm very close to those determined by XRD analysis [33].

3.2. Effect of pH on the Adsorption

The pH of solution has been identified as one of the most important parameter affecting the dyes removal. The effect of pH on the MB removal onto CM-β-CD-Fe_3O_4NPs was examined using batch method. The selected pH range was 2.0–8.0 (Fig. 5). The maximum adsorption percent was observed at pH 6.0. So the remaining all adsorption experiments were carried out at this pH value. The adsorption mechanism may be considered as interaction between adsorbent/adsorbate pair [34, 35]. At highly acidic pH, the active sites of the adsorbent would be occupied by H^+_{aq} ions, which results in lower uptake of MB dye onto CM-β-CD-

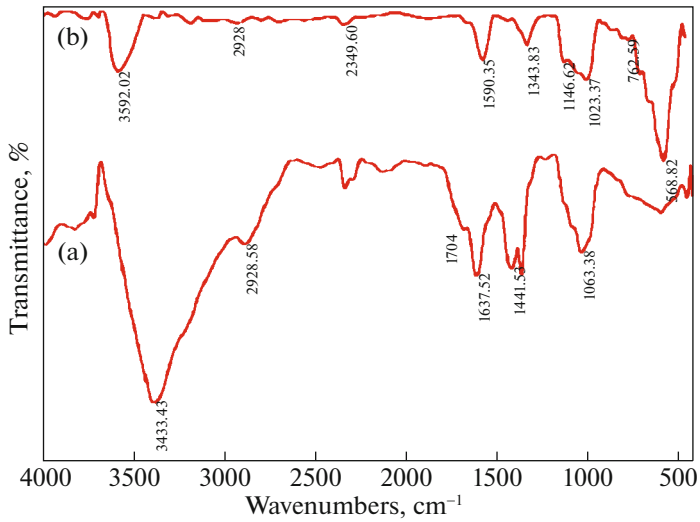

Fig. 2. (a) FT-IR spectrum of CM-β-CD and (b) FT-IR spectrum of the prepared CM-β-CD-Fe_3O_4NPs.

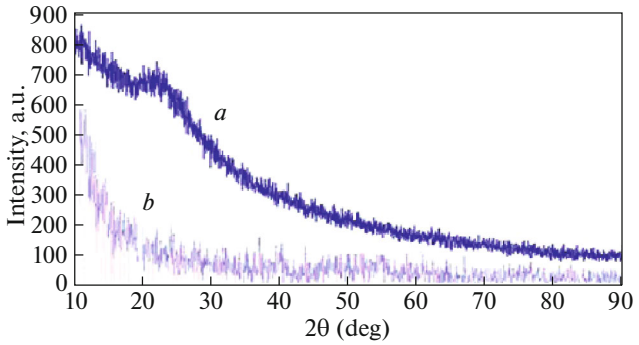

Fig. 3. X-ray diffraction of (*a*) CM-β-CD-Fe_3O_4NPs and (*b*) CM-β-CD.

Fe_3O_4NPs. In turn the adsorbent surface becomes considerably negatively charged as the pH solution increases from 6.0 to higher values which causes in lower up take of MB onto CM-β-CD-Fe_3O_4NPs, so the pH 6.0 is the optimum value in the MB adsorption onto the CM-β-CD-Fe_3O_4NPs adsorbent. Previous research on removing MB onto biomass has been done at pH 6.0 [36].

3.3. Effect of the Adsorbent Dosage

The adsorbent dosage is an important parameter because it determines the capacity of an adsorbent for a given initial concentration of the adsorbate. To examine this effect, the experiments were conducted at several doses (0.10 up to 1.10 g). Figure 6 displays the results. Based on the figure, it may be concluded that dose 0.20 g is a preferred one. The adsorption experiments were done by batch method model. The status of the plot in Fig. 6 can explain by the fact that the adsorption sites on the adsorbent surface remain unsaturated at higher dosage than the optimum dose [36, 37]. When the adsorbent/adsorbate ratio is very small, the available active binding sites are relatively less, so, Ad% becomes low. Therefore, by enhancing the adsorbent/adsorbate ratio, the Ad% increases rapidly and then takes up the gentle changes. This behavior was observed for MB adsorption onto CM-β-CD-Fe_3O_4NPs (see Fig. 6).

3.4. Effect of the Contact Time

The contact time is an effective factor affecting considerably Ad%. Indeed, for maintaining the adsorbent/adsorbate equilibrium, it should enough prolong the contact time for set up the equilibrium between adsorbent and adsorbate. Figure 7 shows the effect of contact time on the Ad% for MB adsorption onto CM-β-CD-Fe_3O_4NPs. Based on this figure, the optimum contact time may be chosen as 45.0 min [38].

3.5. Effect of Temperature

To study the effect of temperature on the adsorption percent of MB dye into CM-β-CD-Fe_3O_4NPs, the experiments were performed at temperatures range of 298.0 to 328.0 K. Figure 8 shows the results. As it can be seen, the Ad% of the process decreases with the temperature increasing. This may be come from the fact that the adsorption process may be exothermic one [38, 39].

3.6. A Comparative Study

The adsorption percent of MB dye onto each of Fe_3O_4NPs, CM-β-CD, and CM-β-CD-Fe_3O_4NPs was evaluated at the optimum condition and the obtained results are represented in Fig. 9. As was can see, the trend of the effectivity of mentioned adsorbents for removing MB from aqueous media was as follow: CM-β-CD-Fe_3O_4NPs (70.0%) > Fe_3O_4NPs (55.0%) > CM-β-CD (43.0%).

3.7. Adsorption Isotherms

Considering the variation of equilibrium adsorption capacities in terms of the equilibrium concentration (C_e) of the adsorbate, under the optimum values of other parameters, we can examine some suitable

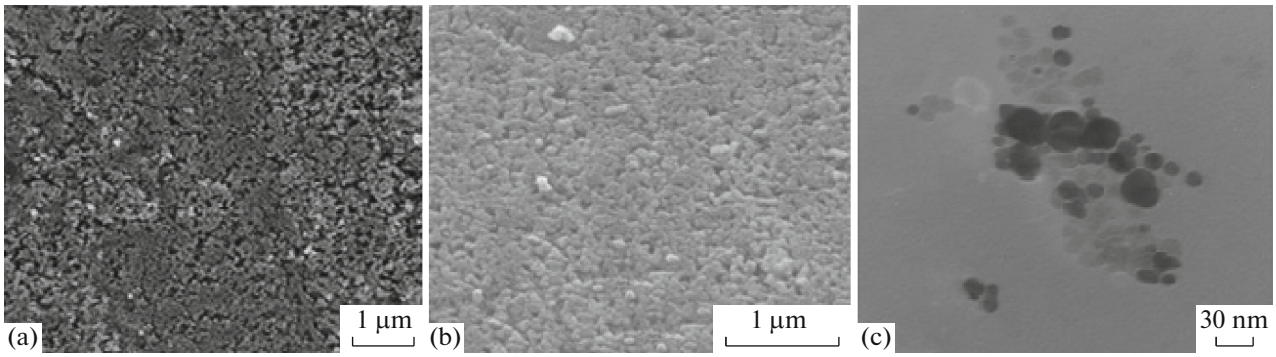

Fig. 4. (a, b) SEM images and (c) TEM pattern of the prepared CM-β-CD-Fe_3O_4NPs.

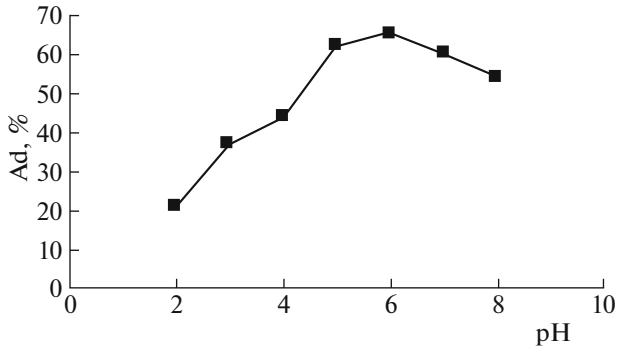

Fig. 5. Effect of initial solution pH on adsorption percentage of MB dye onto CM-β-CD-Fe_3O_4NPs (C_0 = 25.0 mg L^{-1}; dose = 0.20 g; t_c = 45.0 min; stirring speed = 200 rpm; T = 296.0 K).

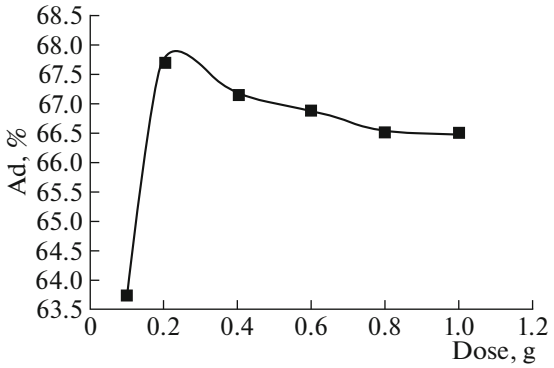

Fig. 6. Effect of CM-β-CD-Fe_3O_4NPs dosage on the adsorption percent of MB dye removing (C_0 = 25.0 mg L^{-1}; pH 6.0; t_c = 45 min; stirring speed = 200 rpm; T = 298.0 K).

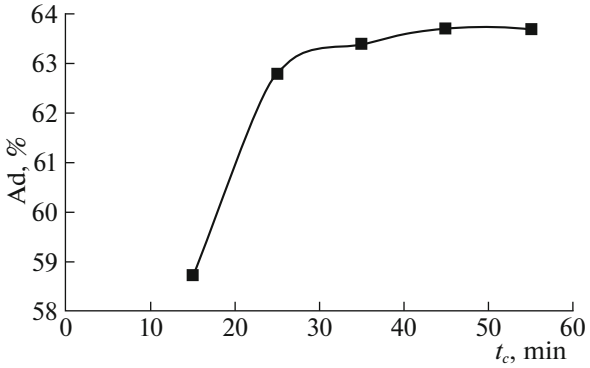

Fig. 7. Effect of contact time on the Ad% respect to the MB adsorption onto CM-β-CD-Fe_3O_4NPs (C_0 = 25.0 mg L^{-1}; pH 6.0; dose = 0.20 g; stirring speed = 200 rpm; T = 298.0 K).

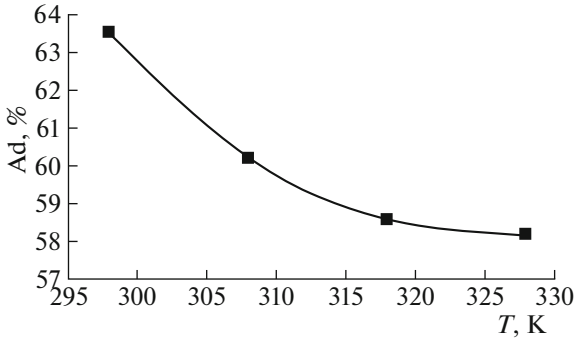

Fig. 8. Effect of temperature on the sorption percent of MB dye adsorption onto CM-β-CD-Fe_3O_4NPs (C_0 = 25.0 mg L^{-1}; pH 6.0; dose = 0.20 g; t_c = 45.0 min; stirring speed = 200 rpm).

isotherms for representing the respect experimental data [40, 41]. To fulfill this goal, we compared the respect experimental results with three most common isotherm models, including Langmuir, Freundlich and Redlich–Peterson isotherms. The nonlinear form of each mentioned model was used for fitting the experimental data (Table 2). The nonlinear Freundlich isotherm fitted better our results (R^2 = 0.9902) than others (R^2 = 0.8912 for Langmuir and R^2 = 0.9827 for Redlich–Peterson). The respect equations for these models are as follows:

$$q_e = \frac{q_m K_L C_e}{1 + K_L C_e}, \quad \text{Langmuir model,} \tag{4}$$

$$q_e = q_m K_F' C_e^{1/n}, \quad \text{Freundlich model,} \tag{5}$$

$$q_e = \frac{AC_e}{1 + BC_e^g}, \quad \text{Redlich-Peterson model,} \tag{6}$$

q_m represents the maximum value of q_e which is necessary for the monolayer covering of the whole surface of the used adsorbent. It may choose $q_m K_F' = K_F$ for Freundlich model. A and B are Redlich–Peterson isotherm constants, and g is the exponent which lies between 0 and 1. The linear equation of the above mentioned models are respectively as:

$$\frac{1}{q_e} = \frac{1}{q_m K_L C_c} + \frac{1}{q_m}, \tag{7}$$

$$\ln q_e = \frac{1}{n} \ln C_e + \ln K_F, \tag{8}$$

$$\ln\left[A \frac{C_e}{q_e} - 1 \right] = g \ln C_e + \ln B. \tag{9}$$

Regarding that the estimation of primary parameters is of the most important, so by changing the primary estimations, the fairly reasonable values of Langmuir isotherm parameters were obtained which are given in Table 2. Based on the R^2 = 0.8912 it is clear that Lang-

muir isotherm can't satisfactorily fit the results of this research.

3.8. The Adsorption Kinetics Survey

Adsorption of a solute by a solid in aqueous solution through complex stages [42] is strongly influenced by several parameters related to the state of the solid (generally with very heterogeneous reactive surface) and to conditions under which the adsorption occurs. The rate of dyes adsorption onto the adsorbent has been fitted to traditional models like, pseudo-first-order and pseudo-second-order models and so on. The Lagergren pseudo-first order model can describe some of the adsorption kinetic data which can be represented as:

$$\frac{dq_t}{dt} = -k_1(q_e - q_t), \tag{10}$$

where q_e an dq_t (mg/g) are the adsorption capacities at equilibrium and at time t, respectively. k_1 is the rate constant of the pseudo-first-order adsorption (min^{-1}). The integrated form of Eq. (10) is:

$$\log(q_e - q_t) = \log q_m - \left(\frac{k_1}{2.303}\right)t. \tag{11}$$

Thus, the slope of $\log(q_e - q_t)$ versus t is equal to $\frac{-k_1}{2.303}$ and the intercept is equal to $\log q_m$ [43].

Pseudo-second-order model is represented as:

$$\frac{dq_t}{dt} = k_2(q_e - q_t)^2, \tag{12}$$

$$\frac{t}{q_t} = \frac{1}{k_2 q_e^2} + \frac{t}{q_e}. \tag{13}$$

The intra-particle-diffusion model is based on the hypothesis that the mechanism of dye removal onto a sorbent material occurs through four steps: (1) bulk diffusion, which is the migration of dye molecules from bulk solution to the surface of the adsorbent, (2) formation the film diffusion, which is diffusion of dye molecules through the boundary layer to the surface of the adsorbent, (3) dye adsorption on the active sites of the surface of the adsorbent, and (4) intra particle diffusion, which is migration of dye molecules to the interior pore structure of adsorbent [31]. The adsorption process is a diffusive mass transfer process where the rate can be expressed in terms of the square root of time (t). The intra-particle-diffusion model can be represented as:

$$q_t = k_i t^{0.5} + I, \tag{14}$$

where k_i is the intra particle diffusion rate constant (mg/g $min^{0.5}$), and I is the effect of boundary layer thickness. The obtained kinetic data for MB adsorption onto CM-β-CD-Fe_3O_4NPs adsorbent were examined with the above mentioned kinetic models

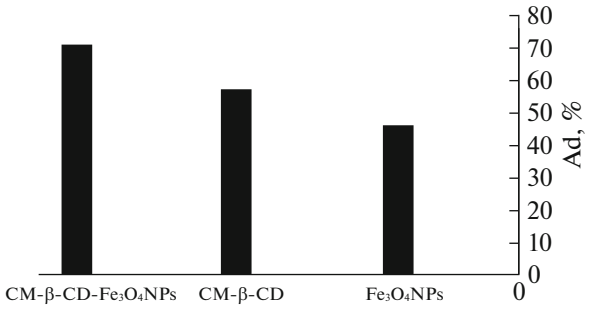

Fig. 9. Comparison of the effectivity of Fe_3O_4NPs, CM-β-CD, and CM-β-CD-Fe_3O_4NPs (C_0 = 25.0 mg L^{-1}; pH 6.0; dose = 0.20 g; t_c = 45.0 min; stirring speed = 200 rpm; T = 298.0 K).

Fig. 10 (Table 3). As, we can see from Fig. 10 the pseudo-second-order model fitted better the kinetic data of this work than others (R^2 = 0.9997) [31, 44, 45].

3.9. Adsorption Thermodynamics

Generally, adsorption thermodynamics is related to definition a conditional equilibrium constant (K_c) as:

$$K_c = q_e/C_e. \tag{15}$$

Therefore, upon determining K_c at a sufficient number of temperatures, then concluding the thermodynamic

Table 2. Calculated various isotherm constants and related correlation coefficients for the adsorption of MB dye onto CM-β-CD-Fe_3O_4NPs adsorbent (C_0 = 5.0–25.0 mg L^{-1}; pH 6.0; dose = 0.20 g; t_c = 45.0 min; stirring speed = 200 rpm; T = 298.0 K)

Langmuir non-linear			
equation	K_L (L/mg)	q_m (mg/g)	R^2
$q_e = \frac{q_m K_L C_e}{1 + K_L C_e}$	1.00	10.00	0.8912
Freundlich non-linear			
equation	K_F (L/mg)	$1/n$	R^2
$q_e = q_m K_F C_e^{1/n}$	0.8814	0.625	0.9902
Redlich–Peterson non-linear			
equation	A (L/g)	B ((L/mg)^g)	G	R^2
$q_e = \frac{AC_e}{1 + BC_e^g}$	0.04	0.05	0.7	0.9827

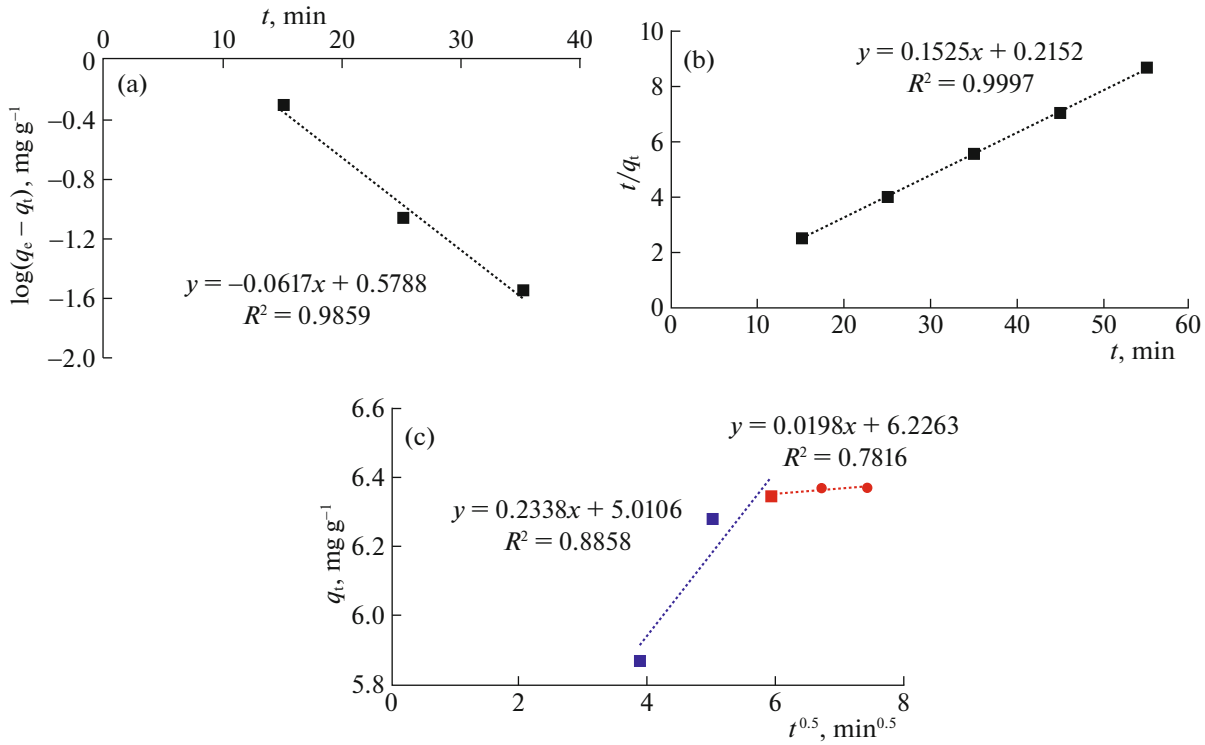

Fig. 10. (a) Pseudo-first-order kinetics plot, (b) pseudo-second-order plot, (c) intra-particle diffusion plot for MB adsorption onto CM-β-CD-Fe_3O_4NPs (C_0 = 25.0 mg L^{-1}; pH 6.0; dose = 0.20 g; stirring speed = 200 rpm; T = 298.0 K; t_c range = 5–55 min).

functions of the adsorption process is quite straightforward. Because:

$$\Delta G^\circ_{ad} = -RT \ln K_c, \quad (16)$$

$$\ln K_c = \frac{\Delta S^\circ_{ad}}{R} - \frac{\Delta H^\circ_{ad}}{RT}, \quad (17)$$

Table 3. Kinetic parameters for the adsorption of MB dye onto CM-β-CD-Fe_3O_4NPs adsorbent

Pseudo- first-order		
k_1 (min^{-1})	q_m (mg/g)	R^2
0.142	1.7833	0.9859
Pseudo-second-order		
k_2 (g/mg min)	q_m (mg/g)	R^2
0.1080	6.5573	0.9997
Intra-particle-diffusion		
$k_{i,1}$ (mg/g $min^{0.5}$)	I_1 (mg/g)	R^2
0.2338	5.0106	0.8858
$k_{i,2}$ (mg/g $min^{0.5}$)	I_2 (mg/g)	R^2
0.0198	6.2263	0.7816

$$\ln\left(\frac{K_{c(2)}}{K_{c(1)}}\right) = -\frac{\Delta H^\circ_{ad}}{R}\left(\frac{1}{T_2} - \frac{1}{T_1}\right), \quad (18)$$

where ΔG°_{ad}, ΔH°_{ad}, and ΔS°_{ad} represent respectively the standard change of Gibbs free energy, enthalpy and entropy associated to the respect adsorption process. T is temperature in Kelvin. In this research, the values of K_c were calculated at 298.0, 308.0, 318.0, and 328.0 K temperatures. The plot of ln K_c versus $(1/T)$ is shown in Fig. 11, from which the values of ΔH°_{ad} and ΔS°_{ad} can be deduced (Table 4). As we can see from Table 4, the values of K_c are greater than 1 at the any used temperature, so, ΔG°_{ad} upon Eq. (16) should be negative indicating that the studied adsorption process is spontaneous in the range of used temperatures, $\Delta H^\circ_{ad} < 0$ indicates that the studies adsorption is exothermic. Based on the magnitude of ΔH°_{ad}, we can say that the mentioned adsorption should be physisorption one and van der Walls interactions are responsible for adsorption taking place. $\Delta S^\circ_{ad} < 0$ indicates a decrease in randomness that occurs during MB adsorption onto CM-β-CD-Fe_3O_4NPs, which may come from the MB aggregation on the CM-β-CD-Fe_3O_4NPs surfaces [46, 47].

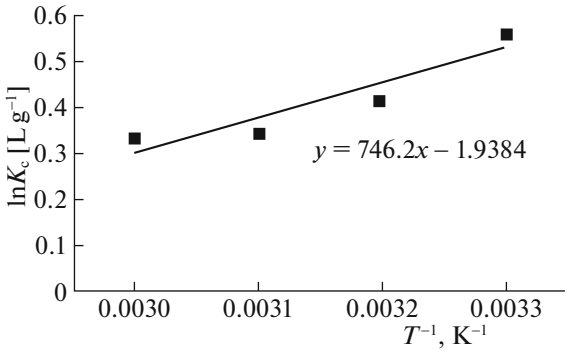

Fig. 11. Plot of ln K_c vs. $1/T$ for MB adsorption onto CM-β-CD-Fe_3O_4NPs which leads to the estimation of the thermodynamic parameters of the process (C_0 = 25.0 mg L^{-1}; pH 6.0; dose = 0.20 g; t_c = 45.0 min; stirring speed = 200 rpm; T range = 298.0–328.0 K).

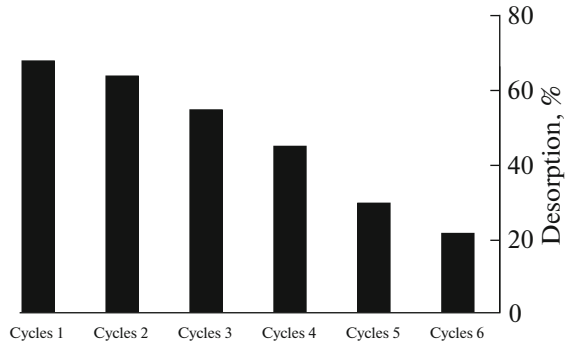

Fig. 12. Desorption of MB dye from CM-β-CD-Fe_3O_4NPs (C_0 = 25.0 mg L^{-1}; pH 6.0; dose = 0.20 g; t_c = 45.0 min; stirring speed = 200 rpm; T = 298.0 K).

3.10. Recycling of the Adsorbent

The ability of recovering and reusing of the adsorbent was tested in several steps of adsorption and the desorption process were done [48]. The results are shown in Fig. 12. As shown in the figure, 68.0% of MB dye was desorbed in the first run and after 6 runs, there were slight changes in MB dye desorption. So, it was concluded that the desired removal of 68% can be achieved after 6 runs.

4. CONCLUSIONS

Synthesized CM-β-CD-Fe_3O_4NPs and its characterization revealed that the synthesized adsorbent has a good ability for MB removing from aqueous media. This synthesized adsorbent was used in various experiments to evaluate the effect of pH, dosage, contact time and temperature on the removal percentage and determining the optimum value of each of them. Consequently, the optimum conditions for conducting the adsorption experiments respect to our present study were fulfilled. So, as a result, we reached to Ad% = 68% at optimum conditions. In general, the effect of pH on Ad% is more important than other effects, because solution pH affects seriously the physicochemical properties of adsorbent and adsorbate, and H^+_{aq} and OH^-_{aq} come into competition with the main adsorbate at low and high pH, respectively. The three most common isotherms (Langmuir, Freundlich, and Redlich–Peterson) were used to fit the related experimental data, but the Freundlich model fitted very effectively our data (R^2 = 0.9902). In addition, the two others were also efficient (R^2 = 0.8912 and 0.9827). Three kinetics equations were used to evaluate, the kinetic behavior of the studied adsorption process. This revealed that the kinetic data of this research is well fitted with pseudo-second-order equation (R^2 = 0.9997). R^2 for pseudo-first-order and intra-particle-diffusion were 0.9859 and 0.8858, respectively. Thermodynamic analysis was considered by introducing a conditional equilibrium constant (K_c) by which estimating the thermodynamic parameters of the adsorption process became possible. The Van't Hoff plot of lnK_c versus ($1/T$) was satisfactory linear. This result allowed us to estimate ΔH°_{ad} and ΔS°_{ad} from the slope and intercept of the plot respectively. ΔG°_{ad} was calculated on the basis of ΔH°_{ad} and ΔS°_{ad} or directly from K_c at each experimental temperature. The MB adsorption onto CM-β-CD-Fe_3O_4NPs was spontaneous ($\Delta G^\circ_{ad} < 0$) and exothermic ($\Delta H^\circ_{ad} < 0$), but with a decrease in randomness ($\Delta S^\circ_{ad} < 0$). Regarding the magnitude of ΔH°_{ad}, we concluded that the studied adsorption in this work is a physical adsorption. As a final result, we should claim that the synthesized CM-β-CD-Fe_3O_4NPs has a good capacity for removing MB dye and the other dyes from aqueous media as a low cost, available and efficient adsorbent.

Table 4. The thermodynamic parameters of MB dye adsorption onto CM-β-CD-Fe_3O_4NPs

C_0, mg/L	T, K	C_e, mg/L	K_c	ΔG°_{ad}, kJ/mol	ΔH°_{ad}, kJ/mol	ΔS°_{ad}, J/mol K
25	298.0	7.29	1.74	–1.377	–6.20	–16.11
	308.0	7.95	1.51	–1.063		
	318.0	8.28	1.42	–1.919		
	328.0	8.37	1.40	–0.899		

ACKNOWLEDGMENTS

We would like to acknowledge Science and Research Branch of Islamic Azad University for supporting this work.

CONFLICT OF INTEREST

The authors declare that they have no conflicts of interest.

REFERENCES

1. V. Rocher, J. M. Siaugue, V. Cabuil, and A. Bee, J. Water Res. **42**, 1290 (2008).
2. S. Hajati, M. Ghaedi, and H. Mazaheri, Desalin. Water Treat. **57**, 3179 (2016).
3. R. Tang, C. Dai, C. Li, W. Liu, S. Gao, and C. Wang, J. Chem. **10**, 1155 (2017).
4. P. Ken Gillman, Psychosomatics **51**, 448 (2010).
5. R. Alizadeh and A. Zeidi, Adv. Environ. Res. **6**, 113 (2017).
6. M. Ghaedi, Sh. Hajati, B. Barazesh, F. Karimi, and Gh. Ghezelbash, J. Ind. Eng. Chem. **19**, 227 (2013).
7. S. M. Lee and S. T. Ong, APCBEE Proc. **9**, 165 (2014).
8. D. Bahadur, D. Dutta, and D. Thakur, Chem. Eng. J. **281**, 482 (2015).
9. K. G. Pavithra, P. S. Kumar, V. Jaikumar, and P. S. Rajan, J. Ind. Eng. Chem. **75**, 1 (2019).
10. Y. Kuang, X. Zhang, and S. Zhou, J. Water. Res. **12**, 587 (2020).
11. D. D. Asouhidou, Colloids Surf. A **346**, 83 (2009).
12. C. Shan, Z. Ma, M. Tong, and J. Ni, Water Res. **69**, 252 (2015).
13. S. Palchoudhury and J. R. Lead, Environ. Sci. Technol. **48**, 14558 (2014).
14. A. Abdilmaleki, S. Mallekpour, and S. Borandeh, RSC Adv. **110**, 1063 (2015).
15. F. Zhao, E. Repo, D. Yin, S. Kalliola, J. Tang, E. Yakovleva, K. C. Tam, and M. Sillanp, Sci. Rep. **10**, 1038 (2017).
16. A. Asfaram and M. Ghaedi, RSC Adv. **6**, 40502 (2016).
17. S. Hajati, M. Ghaedi, B. Barazesh, F. Karimi, R. Sahraei, A. Daneshfar, and A. Asghari, J. Ind. Eng. Chem. **20**, 2421 (2014).
18. K. Kiani, S. Bagheri, and N. Karachi, and E. Alipanahpour Dil, Desalin. Water Treatm. **60**, 1 (2019).
19. K. Boonyarattanakalin, P. Wolschann, P. Toochinda, and L. Lawtrakul, Eur. J. Pharm. Sci. **47**, 752 (2012).
20. U. R. Bhaskara-Amrit, P. Agrawa, and M. Warmoeskerken, Autexj. **11**, 94 (2011).
21. A. S. S. Ibrahim, A. A. Al-Salamah, A. M. El-Toni, M. A. El-Tayeb, and Y. B. Elbadawi, Biol. Electron. J. Biol. **16**, 10 (2013).
22. H. S. Ghazimokri, M. Monajjemi, and H. Aghaie, Rev. Uni. Zulia. **29**, 98 (2020).
23. J. Zhu, P. Wang, and M. Lu, M. J. Braz. Chem. Soc. **24**, 2317 (2013).
24. T. K. Sen, S. Afroze, and H. M. Ang, Equilib., Water Air Poll. **218**, 499 (2011).
25. M. Rafatullah, O. Sulaiman, R. Hashim, and A. Ahmad, J. Hazard. Mater. **177**, 70 (2010).
26. E. Furusaki, Y. Ueno, N. Sakairi, N. Nishi, and S. Tokura, Carbohydr. Polym. **29**, 29 (1996).
27. A. Z. M. Badruddoza, S. S. H. Goh, K. Hidajat, and M. S. Uddin, Colloids Surf., A **367**, 85 (2010).
28. M. R. R. Kooh, M. K. Dahri, L. B. L. Lim, L. H. Lim, and O. A. Malik, Environ Earth Sci. **75**, 783 (2016).
29. M. Auta and B. H. Hameed, J. Chem. Eng. **237**, 350 (2014).
30. W. P. Utomo, E. Santoso, G. Yuhaneka, A. I. Triantini, M. R. Fatqi, M. F. Hudadan, and N. Nurfitria, J. Chem. **13**, 104 (2019).
31. H. S. Ghazi Mokri, N. Modirshahla, M. A. Behnajady, and B. Vahid, Int. J. Environ. Sci. Technol. **12**, 1401 (2015).
32. G. Mamba, X. Y. Mbianda, P. P. Govender, B. B. Mamba, and R. W. Krause, J. Appl. Sci. **10**, 940 (2010).
33. S. Kaur and A. Gaur, Adv. Sci. **20**, 1707 (2014).
34. B. R. Saifutdinov, V. A. Davankov, and M. M. Il'in, Russ. J. Phys. Chem. A **88**, 358 (2014).
35. B. R. Saifutdinov, V. A. Davankov, G. A. Petukhova, M. P. Tsyurupa, Z. K. Blinnikova, and M. M. Il'in, Dokl. Phys. Chem. **462**, 135 (2015).
36. W. Wei, L. Yang, W. H. Zhong, S. Y. Li, J. Cui, and Z. G. Wei, Dig. J. Nanomater. Bios. **10**, 1343 (2015).
37. R. Mahini, H. Esmaeili, and R. Foroutan, Turk. J. Biochem. **24**, 1(2018).
38. D. Pathania, S. Sharma, and P. Singh, Arab. J. Chem. **10**, 1445 (2017).
39. S. Bagheri, H. Aghaei, M. Ghaedi, A. Asfaram, M. Monajemi, and A. A. Bazrafshan, Ultrason Sonochem. **41**, 279 (2018).
40. S. Bagheri, H. Aghaei, M. Ghaedi, M. Monajjemi, and K. Zare, Euras. J. Anal. Chem. **13**, 1 (2018).
41. G. H. Haghdoost, J. Phys. Theor. Chem. **15**, 141 (2019).
42. M. Ghaedi, S. Heidarpour, S. Nasiri, S. Kokhdan, A. Daneshfar, and B. Brazesh, Powder Technol. **228**, 18 (2012).
43. M. Toor and B. Jin, J. Chem. Eng. **187**, 79 (2012).
44. M. Roosta, M. Ghaedi, A. Daneshfar, R. Sahraei, and A. Asghari, Ultrason. Sonochem. **21**, 242 (2014).
45. J. Fu, Z. Chen, M. Wang, S. Liu, J. Zhang, J. Zhang, R. Han, and Q. Xu, Chem. Eng. J. **259**, 53 (2015).
46. M. T. Yagub, T. K. Sen, and H. M. Ang, Water Air Soil Pollut. **223**, 5267 (2012).
47. S. Bagheri, Orient. J. Chem. **32**, 549 (2016).
48. A. A. Sabri, T. M. Albayati, and R. A. Alazawi, Korean J. Chem. Eng. **32**, 1835 (2015).